Cell, Volume *139*

Supplemental Data

Rapid E2-E3 Assembly and Disassembly Enable Processive Ubiquitylation of Cullin-RING Ubiquitin Ligase Substrates

Gary Kleiger, Anjanabha Saha, Steven Lewis, Brian Kuhlman, and Raymond J. Deshaies

Docking of the acidic tail to the Cul1 and Cul5 CTD

Generation of starting models

No crystal structure exists of the Cul1-Rbx1-Cdc34 complex, with or without Nedd8 attached. Additionally, no structure exists of the flexible Cdc34 tail we were interested in modeling. To create the requisite starting models, we used a combination of structural alignments to homologous structures and computational docking.

Cul1-Rbx1-Cd34 was pieced together from PDB files 2OB4 (human Cdc34) and 1LDJ (Cul1-Rbx1) (Zheng et al., 2002). Cul1 was trimmed to residues 411-776. To approximate the E2–RING interaction, these two PDB files were aligned against the E2–RING complex CBL-UBCH7, 1FBV (Zheng et al., 2000). This docking alignment was then refined using Rosetta's docking tools (Gray et al., 2003). A similar model complex was generated in the same fashion from PDB files 2OB4 (Cdc34) and 3DQV (chains A, C, and R) (Cul5-Rbx1-Nedd8) (Duda et al., 2008).

The final step of generating starting models was attaching the tail sequence to Cdc34 (not seen in the crystal structure). We used the simple expedient of extending the tail straight out into space from the C-terminal residue in the Cdc34 crystal structure.

Modeling the flexible tail

To explore how the flexible tail might interact with the E3 in this system, we built a new protocol within the Rosetta framework. Figure (S8) demonstrates

the flow of this protocol. The protocol has a reduced-representation “centroid” phase and a second refinement phase with all atoms present.

The centroid phase is designed to collapse the long tail, which initially points straight into space, into some reasonable conformation. The reduced representation has only single large “centroid” atoms replacing the side-chains (Rohl et al., 2004), obviating the need to consider packing details. The advantage of using this representation in the early part of the trajectory is that we no longer need to repack side-chains to smooth out minor side-chain/side-chain clashes, thus speeding up the computation. This phase consisted of 5,000 Metropolis Monte Carlo cycles. Most cycles were used to perturb the tail structure with one of three Rosetta tools (Rohl et al., 2004).

The first tool, marked as Small_180 on Figure S8, randomly perturbed a phi and psi angle of a tail residue, weighted to choose good Ramachandran values. The second, Shear_180 on Figure S8, modifies a phi angle at position n and psi at position n-1 in opposite directions. This has the effect of tweaking local structure without longer-distance effect. Again, this was a random perturbation subject to Ramachandran constraints. Shear movements are designed to minimize perturbation of the backbone far from the move, so they were disabled for the first third of the protocol to give the tail a chance to develop interactions before their use.

The third type of perturbation was a 3-residue fragment insertion. Fragment insertion consists of replacing the backbone torsional parameters with parameters from a small protein fragment derived from the PDB. Fragments were generated via the Robetta server (Kim et al., 2004). This allowed for somewhat faster sampling of local conformational and secondary structure preferences.

After 19 cycles, the protocol performed a gradient-based energy minimization of the structure. The available degrees of freedom were the backbone torsion angles phi, psi and omega of tail residues (the same freedoms perturbed in the other steps). The score function used in this phase contained terms for van der Waals repulsion, hydrogen bonding, electrostatics,

Ramachandran, and residue-pair potentials (which incorporate van der Waals attraction and solvation) (Rohl et al., 2004).

After 5,000 perturbing cycles, the lowest-scoring structure seen in the trajectory was recovered. Side-chains were returned to this structure. The crystallographic side-chains were used outside the tail. One of Rosetta's default full atomic representation energy functions, score12, was used for scoring in this phase (Kuhlman et al., 2003) (Smith and Kortemme, 2008). The tail region and any side-chains within 10 Ångstroms of the tail were subjected to a combinatorial repacking wherein a Monte Carlo procedure chose low-energy side-chain conformations from the full set of available rotamers. The side-chains and the tail backbone torsions were then energy minimized. The refinement phase ran for 3,000 cycles of Metropolis Monte Carlo optimization. Most cycles consisted of a random small perturbation. These perturbations were small or shear movements as before, except the perturbation was constrained to within 4 degrees, instead of anywhere in Ramachandran space. This sort of perturbation was immediately followed by a single-pass random-order rotamer optimization of the tail and its neighbors (rotamer trials). After 14 cycles, a minimization of the tail side-chains, tail backbone torsions, and side-chains neighboring the tail was performed. Another 14 cycles after that, a full combinatorial repacking operation was performed before the minimization. At the end of each trajectory, the best structure recorded was reported as output.

The protocol as a whole was run for approximately 30,000 trajectories per experiment, which is slightly more than 1,000 processor-days on a 2.3 GHz chip. It is customary to run extremely large numbers of trajectories when doing structure prediction with Rosetta. The random nature of Monte Carlo sampling means that trajectories will sometimes get trapped in poor minima, so many trajectories are needed to sufficiently sample the structure space.

Sorting models

To search through our dataset for models that addressed the question of how the E2 might bind the E3, we sorted models based on E2-E3 binding energy. This was calculated as the complex score minus the scores of the E2

and E3-RING (±Nedd8) in isolation. It should be noted that there are two components to this binding energy. There is a constant component represented by the direct, canonical E2-RING interaction. This interaction was optimized by docking as a precursor step but not modified during the main part of the protocol. The second interaction represents binding between the E2 tail and the body of the E3.

Supplemental References

Duda, D.M., Borg, L.A., Scott, D.C., Hunt, H.W., Hammel, M., and Schulman, B.A. (2008). Structural insights into NEDD8 activation of cullin-RING ligases: conformational control of conjugation. Cell *134*, 995-1006.

Gray, J.J., Moughon, S., Wang, C., Schueler-Furman, O., Kuhlman, B., Rohl, C.A., and Baker, D. (2003). Protein-protein docking with simultaneous optimization of rigid-body displacement and side-chain conformations. J Mol Biol *331*, 281-299.

Kim, D.E., Chivian, D., and Baker, D. (2004). Protein structure prediction and analysis using the Robetta server. Nucleic Acids Res *32*, W526-531.

Kuhlman, B., Dantas, G., Ireton, G.C., Varani, G., Stoddard, B.L., and Baker, D. (2003). Design of a novel globular protein fold with atomic-level accuracy. Science *302*, 1364-1368.

Larkin, M.A., Blackshields, G., Brown, N.P., Chenna, R., McGettigan, P.A., McWilliam, H., Valentin, F., Wallace, I.M., Wilm, A., Lopez, R.*, et al.* (2007). Clustal W and Clustal X version 2.0. Bioinformatics *23*, 2947-2948.

Rohl, C.A., Strauss, C.E., Misura, K.M., and Baker, D. (2004). Protein structure prediction using Rosetta. Methods Enzymol *383*, 66-93.

Saha, A., and Deshaies, R.J. (2008). Multimodal activation of the ubiquitin ligase SCF by Nedd8 conjugation. Mol Cell *32*, 21-31.

Smith, C.A., and Kortemme, T. (2008). Backrub-like backbone simulation recapitulates natural protein conformational variability and improves mutant side-chain prediction. J Mol Biol *380*, 742-756.

Zheng, N., Schulman, B.A., Song, L., Miller, J.J., Jeffrey, P.D., Wang, P., Chu, C., Koepp, D.M., Elledge, S.J., Pagano, M.*, et al.* (2002). Structure of the Cul1-Rbx1-Skp1-F boxSkp2 SCF ubiquitin ligase complex. Nature *416*, 703-709.

Zheng, N., Wang, P., Jeffrey, P.D., and Pavletich, N.P. (2000). Structure of a c-Cbl-UbcH7 complex: RING domain function in ubiquitin-protein ligases. Cell *102*, 533-539.

Supplemental Figure Legends

Figure S1. Multiple Sequence Alignment of the human Cdc34a, human Cdc34b, and yeast Cdc34 1 - 230 sequences. While the yeast Cdc34 sequence is 295 amino acids, 1 – 230 was included during the alignment procedure (MUSCLE) and resulted in a better alignment than when the full-length sequence was used. Amino acids within the catalytic domain are shaded olive. Amino acids within the acidic tail domain are shaded light-blue. Acidic residues in the tail domain are shaded yellow.

Figure S2. The effects of Cul1 neddylation and ubiquitin oxyesterification to Cdc34 on k_{on} are less than 2-fold. All experiments were performed identically to those in Figure 1a. (A) Measurement of k_{off} for Lumio Green labeled WT Cdc34 and neddylated RC^{CFP} complex. k_{on} was estimated from k_{off} and K_d was taken from (Saha and Deshaies, 2008). (B) Measurement of k_{off} for WT Cdc34 that was oxyestified to ubiquitin and neddylated RC^{CFP} complex. k_{on} was estimated from k_{off} and K_d was taken from (Saha and Deshaies, 2008). (C) Measurement of k_{off} for WT Cdc34 and a full $SCF^{\beta TrCP}$ complex. Equimolar βTrCP-Skp1 was added to the Lumio Cdc34-RC^{CFP} complex. Notice that the value of k_{off} is very nearly the same whether the full SCF complex is assembled or not (27 and 35 sec^{-1}, respectively). The ionic strength of the reaction buffer for all experiments was 50 mM.

Figure S3. Binding assays to RC^{CFP} with N-terminally labeled Lumio Green Cdc34 protein show similar results as when the Lumio tag is at the C-terminus. (A) Salt sensitivity of FRET efficiency of RC^{CFP} complex saturated with C-terminally labeled WT Cdc34 (white bars) or RC^{CFP} complex with nearly saturating N-terminally labeled WT Cdc34 (black bars). Notice that N-terminally labeled Cdc34-RC^{CFP} complex is highly salt sensitive, similar to C-terminally labeled Cdc34. (B) Salt sensitivity of Δ221 Cdc34. (C) Titration of N-terminal Lumio-labeled Cdc34 on RC^{CFP}. All experiments were done in duplicate.

Figure S4. (A) Model showing the interaction between the acidic tail and the Cul5 CTD(Nedd8)-Rbx1 structure. Cul5, Rbx1 and Nedd8 are colored according to the electrostatic potential of the surface. The location of Nedd8 in the structure is shown by the dashed gray oval. The catalytic domain of Cdc34 is shown as a yellow ribbon diagram. Cdc34 residues in the tail are yellow ball-and-sticks, except acidic residues are colored red. (B) Magnified view of (A).

Figure S5. Neddylation of KKR SCF results in a similar degree of activation as WT SCF. (A) Time course of the neddylation of WT or KKR RC. Notice that at completion the same amount of product is observed for either WT or KKR RC. (B,C) Ubiquitylation of a mono-ubiquitylated β-Catenin peptide by either WT (B) or KKR (C) SCF and 0.5 μM WT Cdc34. Neddylation stimulated the rate of substrate consumption under multi-turnover conditions by approximately 2-fold for both WT and KKR SCF.

Figure S6. Multiple sequence alignment of 9 cullin sequences by MUSCLE. Coloring of conserved residues was performed according to definitions in ClustalX (Larkin et al., 2007). Black asterisks were placed beneath positions in the MSA corresponding to human Cul1 KR claw residues 431, 432, 435, 678, 679 and 681.

Figure S7. Cdc34-Δ190 can be fully thioesterified to ubiquitin at concentrations as high as 100 μM. SDS-PAGE in the absence of reducing reagent for reactions containing human E1, various concentrations of human Cdc34-Δ190 (shown), and ubiquitin. The location of apo-E2 and the thioesterified E2-ubiquitin complex are shown. Notice that concentrations as high as 100 μM E2 can be achieved where little or no apo-E2 is present.

Figure S8. Flow diagram illustrating the procedure used for modeling the Cdc34 acidic tail interaction with either Cul1 or neddylated Cul5 CTD.

Table S1. Constructs, expression, and purification for proteins used in this manuscript.

Protein	Construct	Strain	Expression	Purification	Comments
WT hCdc34[a]	pET11b-hCdc34-His6	RDB2314	E.coli	NiNTA[b]->S75[c]	
Δ190 hCdc34	pET11b-Δ190 hCdc34-His6	RDB2315	E.coli	NiNTA->S75	
NLum[d]-WT hCdc34	pET11b-Lum-hCdc34-His6	RDB2316	E.coli	niNTA->S75	
CLum-WT hCdc34	pET11b-hCdc34-Lum-His6	RDB2317	E.coli	niNTA->S75	
CLum-Δ221 hCdc34	pET11b-Δ221 hCdc34-Lum-His6	RDB2318	E.coli	niNTA->S75	
C227S hCdc34	pET11b-C227S-hCdc34-His6	RDB2319	E.coli	niNTA->S75	
UbcH5c	pGex-TEV-UbcH5c	RDB1973	E.coli	GST->TEV digest (on beads)->S75	
Cul1 NTD Rbx1-Cul1 CTD	pAL Cul1 NTD, pCool Rbx1 Cul1 CTD	RDB2080 RDB2081	E.coli	GST-Thrombin-Mono S->S200[e]	Co-expression
Cul1 NTD Rbx1-Cul1 CTD (CFP)	pAL Cul1 NTD, pCool Rbx1 Cul1 CTD (CFP)	RDB2080 RDB2228	E.coli	GST-Thrombin-Mono S->S200	Co-expression
Cul1 NTD Rbx1-Cul1 CTD K679C	pAL Cul1 NTD, pCool Rbx1 Cul1 CTD K679C	RDB2320	E.coli	GST-Thrombin-Mono S->S200	Co-expression
Cul1 NTD Rbx1-Cul1 CTD KKR	pAL Cul1 NTD, pCool Rbx1 Cul1 CTD KKR	RDB2321	E.coli	GST-Thrombin-Mono S->S200	Co-expression
Δ230 yCdc34[f]	pET11b-Δ230 yCdc34-His6	RDB2322	E.coli	Ni-NTA->S75	
Δ210 yCdc34	pET11b-Δ210 yCdc34-His6	RDB2323	E.coli	Ni-NTA->S75	
βTrCP-Skp1 (139-569)	GST βTrCP-Skp1	-	Hi5 insect cell	GST->Thrombin-Mono Q->S200	Co-expression
ySCF (Hrt1, Cdc53, Skp1, Cdc4)		-	Hi5 insect cell	Py beads	Co-expression

[a] human, [b] Nickel agarose purification, [c] Superdex 75 gel filtration column
[d] CCPGCC Lumio tag sequence, [e] Superdex 200 gel filtration column, [f] yeast

Table S2. Reaction conditions for ubiquitylation assays in this manuscript

Figure	E1	Ub	E2	SCF	Substrate	Competitor
2a	hE1, 1 μM	60 μM	WT Cdc34 (titration series)	WT Cul1-N8, Rbx1, Skp1, βTrCP (0.15 μM)	$\beta Catenin^{Ub}$ peptide (4 μM)	
2b	hE1, 1 μM	150 μM	Δ190 Cdc34 (titration series)	WT Cul1-N8, Rbx1, Skp1, βTrCP (0.15 μM)	$\beta Catenin^{Ub}$ peptide (4 μM)	
5a	hE1, 1 μM	60 μM	WT Cdc34 (titration series)	KKR Cul1, Rbx1, Skp1, βTrCP (0.1 μM)	$\beta Catenin^{Ub}$ peptide (3 μM)	
5b	hE1, 1 μM	60 μM	Δ190 Cdc34 (9 μM)	WT Cul1, Rbx1, Skp1, βTrCP (0.4 μM)	$\beta Catenin^{Ub}$ peptide (3 μM)	
5b	hE1, 1 μM	60 μM	Δ190 Cdc34 (9 μM)	KKR Cul1, Rbx1, Skp1, βTrCP (0.4 μM)	$\beta Catenin^{Ub}$ peptide (3 μM)	
5c	hE1, 1 μM	60 μM	Ubc5c (0.75 μM)	WT Cul1, Rbx1, Skp1, βTrCP (0.2 μM)	βCatenin peptide (5 μM)	
5c	hE1,1 μM	60 μM	Ubc5c (0.75 μM)	KKR Cul1, Rbx1, Skp1, βTrCP (0.2 μM)	βCatenin peptide (5 μM)	
5d	yE1, 1 μM	300 μM	Δ230 yCdc34 (10 μM)	ySCF (0.35 μM)	Cyclin E peptide (30 nM)	Cyclin E peptide (20 μM)
5d	yE1, 1 μM	300 μM	Δ210 yCdc34 (10 or 100 μM)	ySCF (0.35 μM)	Cyclin E peptide (30 nM)	Cyclin E peptide (20 μM)

Figure S1


cdc34|Yeast|/1-230 1 -MSSRKSTASSLLLRQYRELTDPKKAIPSFHIELED 35
ubc3-a/1-236 1 MARPLVPSSQKALLLELKGLQE--EPVEGFRVTLVD 34
UBC3B|HomoSapiens|/1-238 1 MAQQQMTSSQKALMLELKSLQE--EPVEGFRITLVD 34
cdc34|Yeast|/1-230 36 DSNIFTWNIGVMVLNEDSIYHGGFFKAQMRFPEDFP 71
ubc3-a/1-236 35 EGDLYNWEVAIFG-PPNTYYEGGYFKARLKFPIDYP 69
UBC3B|HomoSapiens|/1-238 35 ESDLYNWEVAIFG-PPNTLYEGGYFKAHIKFPIDYP 69
cdc34|Yeast|/1-230 72 FSPPQFRFTPAIYHPNVYRDGRLCISILHQS-GDPM 106
ubc3-a/1-236 70 YSPPAFRFLTKMWHPNIYETGDVCISILHPPVDDPQ 105
UBC3B|HomoSapiens|/1-238 70 YSPPTFRFLTKMWHPNIYENGDVCISILHPPVDDPQ 105
cdc34|Yeast|/1-230 107 TDEPDAETWSPVQTVESVLISIVSLLEDPNINSPAN 142
ubc3-a/1-236 106 SGELPSERWNPTQNVRTILLSVISLLNEPNTFSPAN 141
UBC3B|HomoSapiens|/1-238 106 SGELPSERWNPTQNVRTILLSVISLLNEPNTFSPAN 141
cdc34|Yeast|/1-230 143 VDAAVDYRK------NPEQYKQRVKMEVERSKQDIP 172
ubc3-a/1-236 142 VDASVMYRKWKESKGKDREYTDIIRKQVLGTKVDAE 177
UBC3B|HomoSapiens|/1-238 142 VDASVMFRKWRDSKGKDKEYAEIIRKQVSATKAEAE 177
cdc34|Yeast|/1-230 173 K-GFIMPTSESAYISQSKLDEPESNKDMADNFWYDS 207
ubc3-a/1-236 178 RDGVKVPTTLAEYCVKTKAPAPDEGSDLFYDDYYED 213
UBC3B|HomoSapiens|/1-238 178 KDGVKVPTTLAEYCIKTKVPSNDNSSDLLYDDLYDD 213
cdc34|Yeast|/1-230 208 DLDD---DENGSVILQDDDYDDGNNH- 230
ubc3-a/1-236 214 G-EV---EEEADSCFGDDEDDSGTEES 236
UBC3B|HomoSapiens|/1-238 214 DIDDEDEEEEDADCY--DDDDSGNEES 238

Figure S2

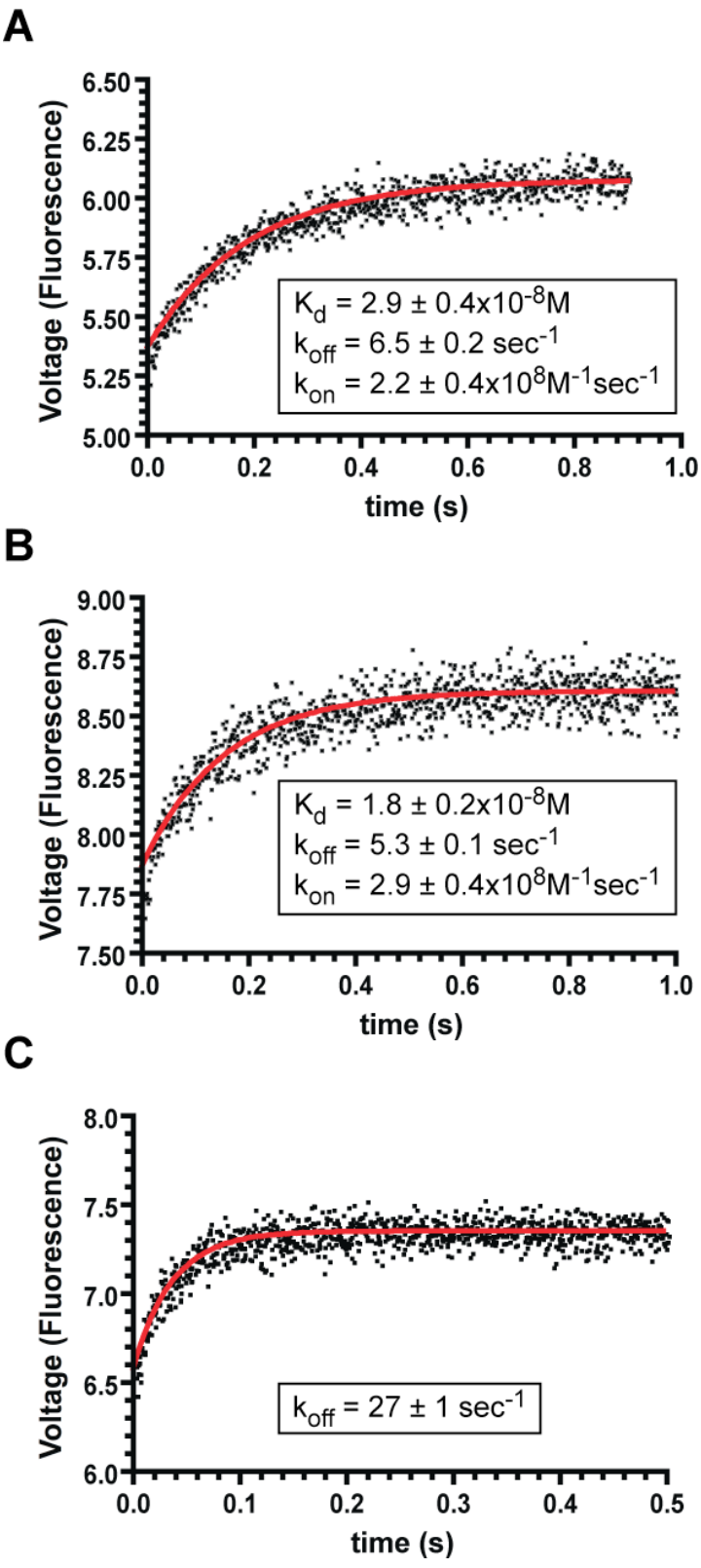
A
Voltage (Fluorescence)
time (s)
K_d = 2.9 ± 0.4x10^{-8}M
k_{off} = 6.5 ± 0.2 sec^{-1}
k_{on} = 2.2 ± 0.4x10^{8}M^{-1}sec^{-1}
B
Voltage (Fluorescence)
time (s)
K_d = 1.8 ± 0.2x10^{-8}M
k_{off} = 5.3 ± 0.1 sec^{-1}
k_{on} = 2.9 ± 0.4x10^{8}M^{-1}sec^{-1}
C
Voltage (Fluorescence)
time (s)
k_{off} = 27 ± 1 sec^{-1}

Figure S3

A

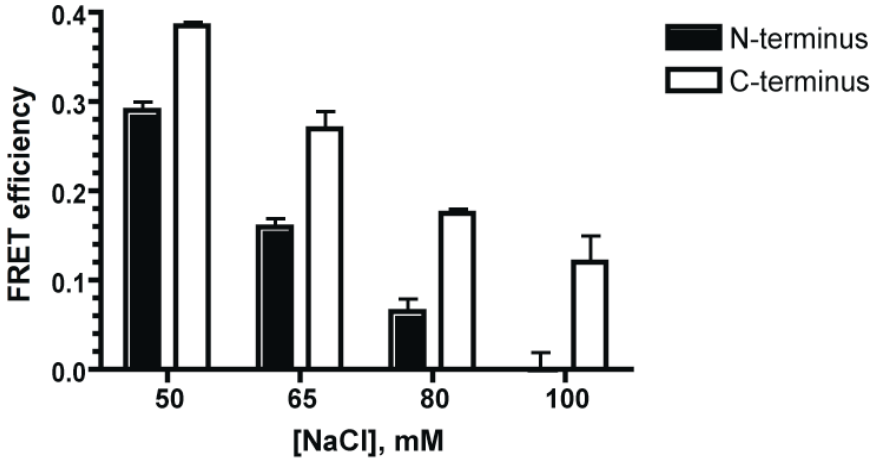

B

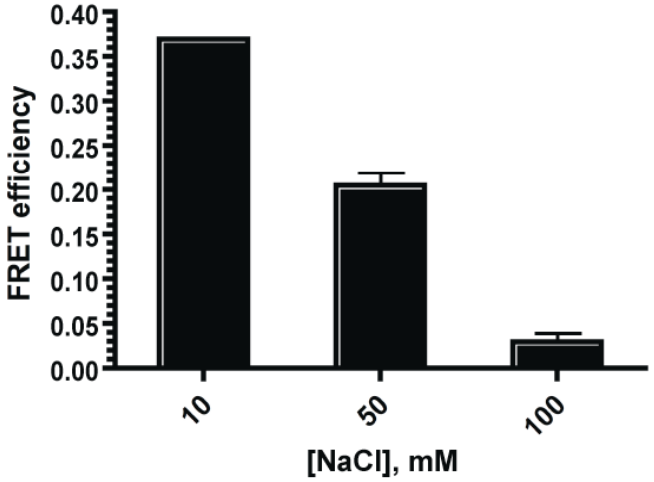

C

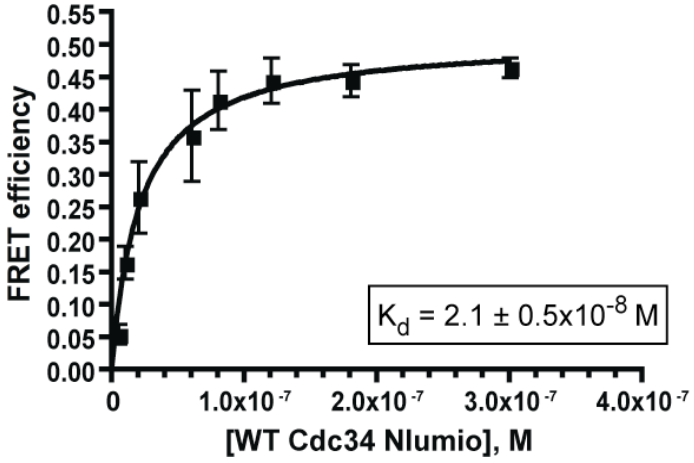

Figure S4

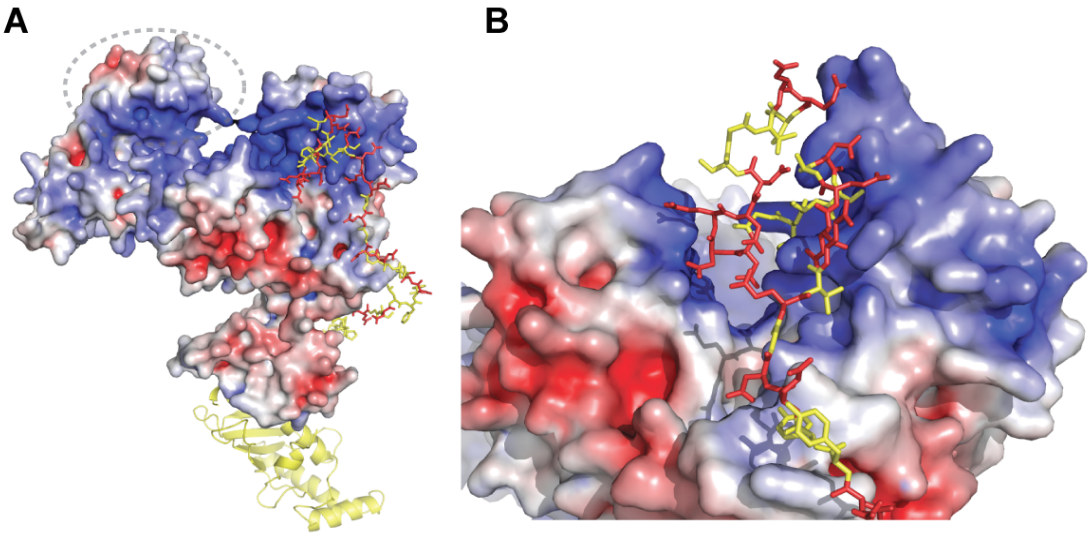

Figure S5

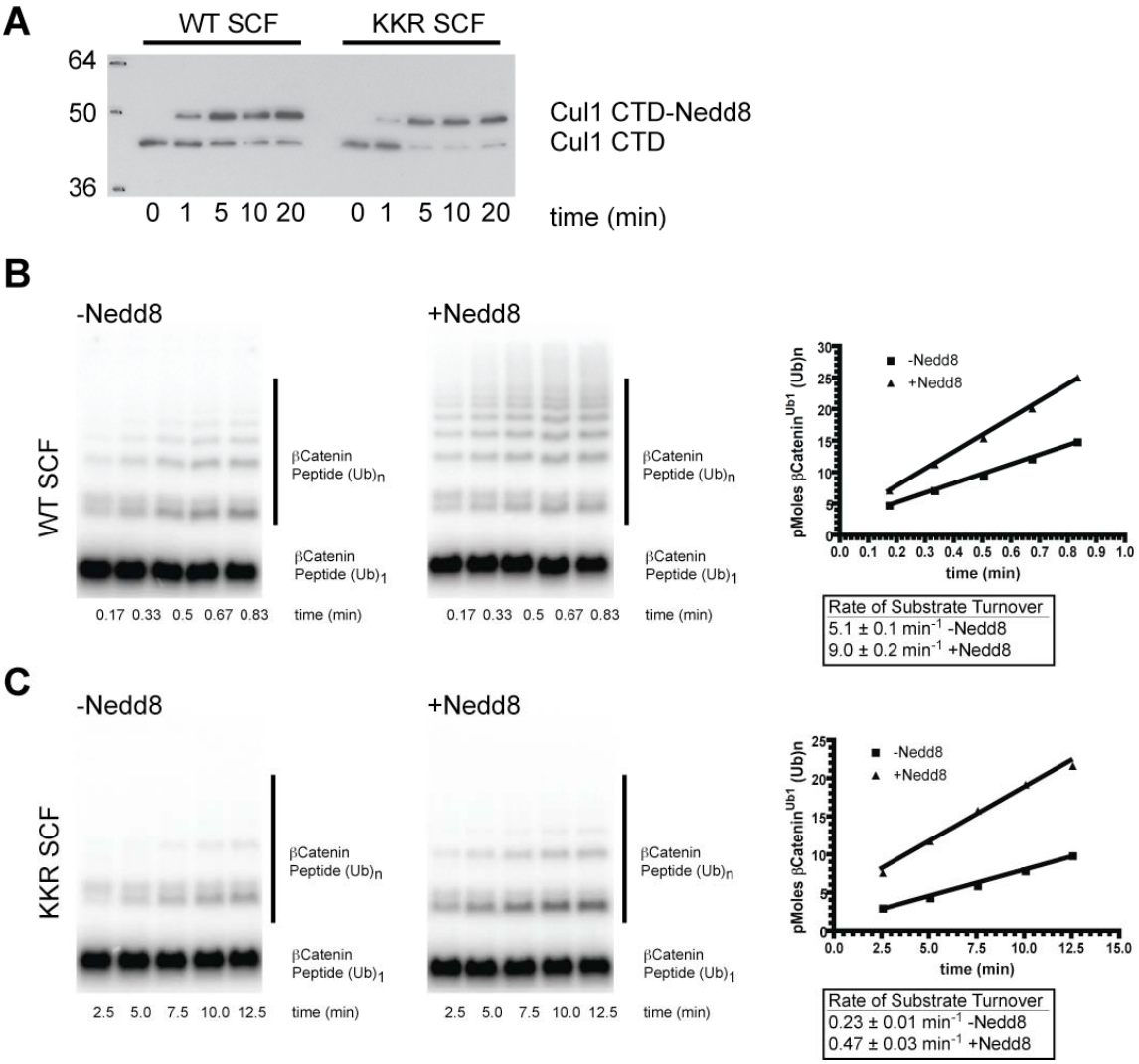
A
WT SCF
KKR SCF
64
50
36
0 1 5 10 20 0 1 5 10 20
Cul1 CTD-Nedd8
Cul1 CTD
time (min)
B
-Nedd8
+Nedd8
WT SCF
βCatenin Peptide (Ub)n
βCatenin Peptide (Ub)1
0.17 0.33 0.5 0.67 0.83 time (min)
pMoles βCatenin Ub1 (Ub)n
time (min)
Rate of Substrate Turnover
5.1 ± 0.1 min-1 -Nedd8
9.0 ± 0.2 min-1 +Nedd8
C
KKR SCF
2.5 5.0 7.5 10.0 12.5 time (min)
Rate of Substrate Turnover
0.23 ± 0.01 min-1 -Nedd8
0.47 ± 0.03 min-1 +Nedd8

Figure S6

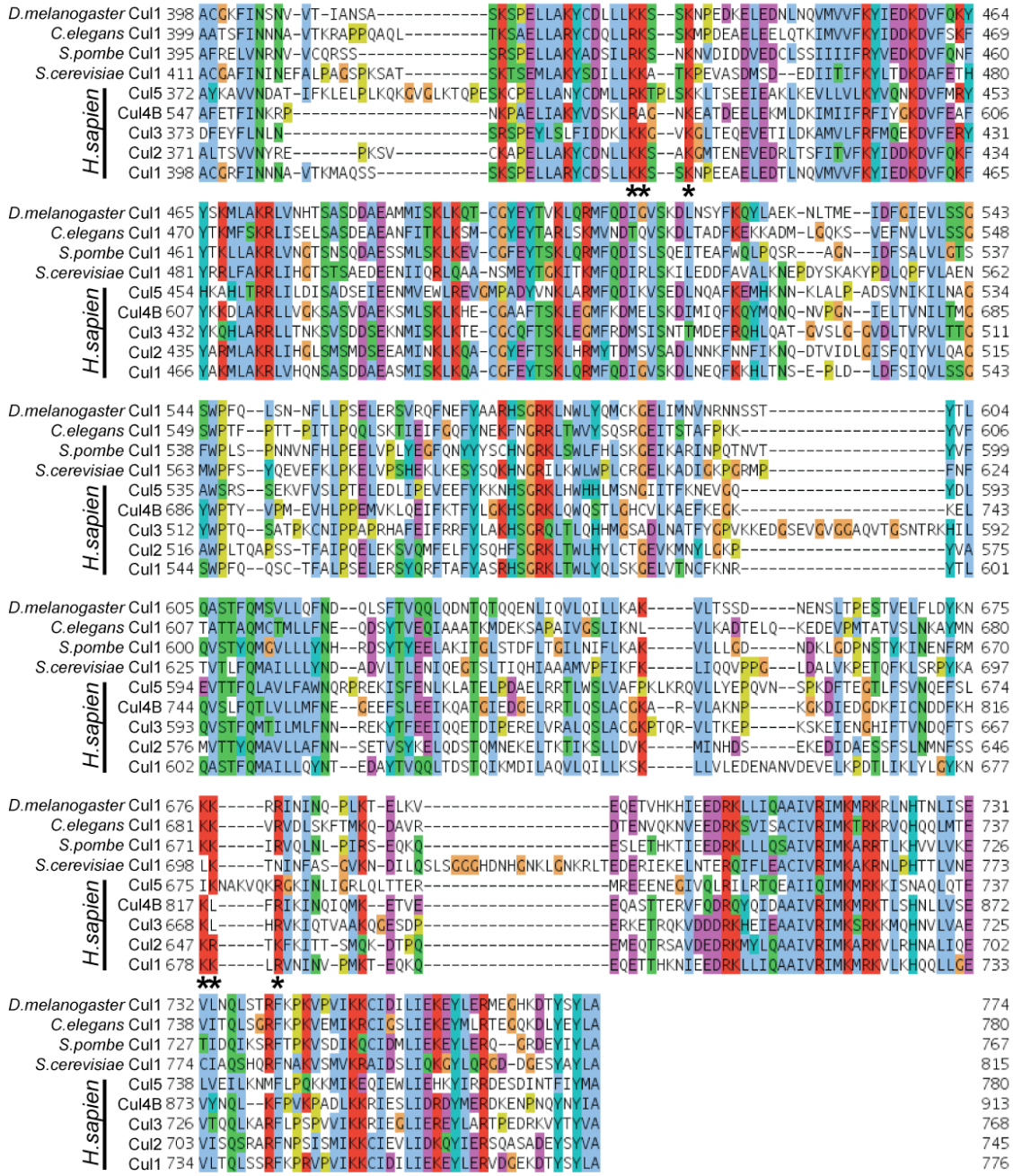
D.melanogaster Cul1
C.elegans Cul1
S.pombe Cul1
S.cerevisiae Cul1
H.sapien
Cul5
Cul4B
Cul3
Cul2
Cul1

Figure S7

A

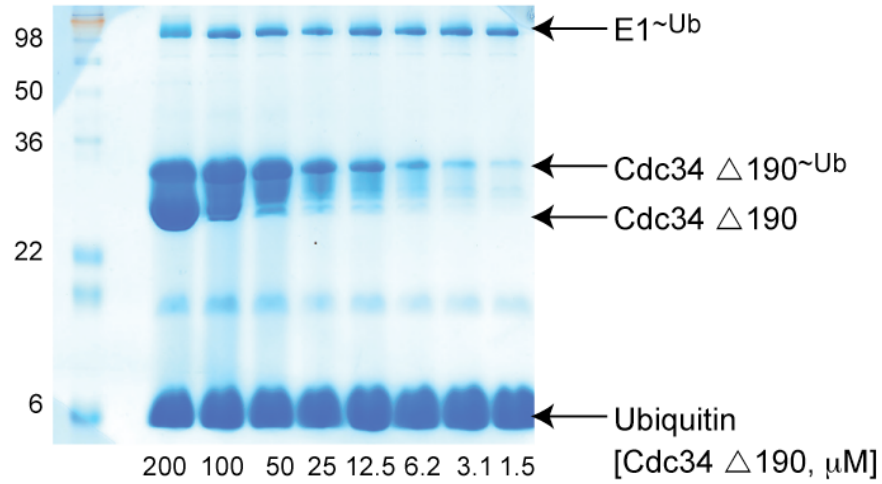

Figure S8